Structure of the water molecule layer between ice and amorphous/crystalline surfaces based on molecular dynamics simulations

Shota Uchida†‡, Kunio Fujiwara†§, Masahiko Shibahara†*

**sh.uchida@screen.co.jp*, +81-75-931-7925

†Department of Mechanical Engineering, Graduate School of Engineering, Osaka University, 2-1 Yamadaoka, Suita, Osaka 565-0871, Japan

‡R & D Department, SCREEN Holdings Co., Ltd., 322 Furukawa-cho, Hazukashi, Fushimi-ku, Kyoto, Kyoto 612-8486, Japan

§Japan Science and Technology Agency, PRESTO, Saitama 332-0012, Japan

KEYWORDS

molecular dynamics, water molecules, ice-silica interface, ice crystal

ABSTRACT

The structure of the water layer between the ice interface and the hydroxylated amorphous/crystalline silica surfaces was investigated using molecular dynamics simulations. The results indicate that the density profile in the direction perpendicular to the surface has two density peaks in the water layer at the ice-silica interface, which are affected by the silanol group density on the wall and the degree of supercooling in the system. In the two density peaks, the one facing the ice interface side has the same structure as the ice crystal while the other density peak facing the silica surface has an ice-like structure. In the solidification process, the ice and ice-like structuring in the layer progresses more on the amorphous silica surface where the density of the silanol groups is low. The relationship between the ice crystallization and thickness of the layer has been studied in detail; the lower the temperature, the more the ice crystallization progresses and the thinner the layer becomes.

INTRODUCTION

Ice crystal surfaces covered by a layer of premelted ice, which is formed by the disordering of water molecules, are generally known as a quasi-liquid layer (QLL). Gaining an understanding of the QLL is crucial to obtaining insights on various physical phenomena (1, 2), such as reduction of ice friction (3), control of adhesion (4), and climate change (5). In recent years, ice phase change phenomenon has found applications in semiconductor manufacturing processes as a new cleaning method for semiconductor structures with sizes of a few nanometers (6–9).

Previous studies have carried out several experimental investigations (10,11) to characterize the properties and thickness of the QLL. To reveal the thickness and the structure of the QLL at the substrate-ice interface, several experimental methods have been applied, such as ellipsometry (12), X-ray diffraction (13–15), reflectivity (16), atomic force microscopy (AFM) (17,18), in-situ transmission electron microscopy (TEM) observation (19,20), optical microscopy (21), and neutron diffraction (22). In particular, numerous experimental data have been collected for ice-silica interfaces, viz., the thickness (16) and interfacial water structure (23, 24) of a QLL on hydroxylated silica film, mesoporous silica (25), and nanoporous MCM-41 (26). These studies have confirmed that the QLL thickness on the silica surface is approximately 1 nm at 10 K degree of supercooling, and that the QLL has an ice-like structure depending on the temperature and humidity. These studies also suggested that an ice-like structure was created by hydrogen bonds formed between water molecules and silanol groups on the hydroxylated silica surface. However, it is still difficult to experimentally observe the detailed structure of the QLL with a thickness of few nanometers on the molecular scale.

Several simulations have been conducted on the dynamics of water molecules during the solidification process. Molecular dynamics simulations could provide details on the microscopic

behavior of molecules, which would allow us to observe the details of the solidification process (27, 28), such as the QLL thickness of the ice–vapor interface (29), crystallization in nanochannels (30–32), and ice nucleation on nanostructure (33). In addition, numerous computational studies have been conducted on the dynamics of water on the silica wall surface, such as diffusivity (34) and tessellation (35), the effects of silanol groups on water molecules (36), contact angles (37–39), and adsorption in nanopores (40). The effect of the hydrogen bonds on the dynamics of water molecules near the wall surface was confirmed on hard (41) and soft (42) surfaces and it has been studied in addition to the hydrogen bonds between the silica wall surface and water (43,44). These studies have confirmed that the density profile and diffusivity of the vapor–ice interface change according to the degree of supercooling and suggested that the hydrogen bonds formed between water molecules affect these phenomena. However, few studies have investigated the detailed structure of the QLL at the silica-ice interface on the nanometer scale.

From the experimental and computational perspectives, the molecular scale structure of water molecules in the layer between ice and silica surfaces is still not clear.

The purpose of this study is to provide the molecular details of the structure of the water layer between the silica surface and the ice solidification interface using non-equilibrium molecular dynamics simulations. Simulations were conducted for a coexistence system of water and ice on hydroxylated crystalline and amorphous silica surfaces. We investigated the density profile and structure of water molecules in the vicinity of the two types of walls, before and after the solidification interface connected. Furthermore, we examined the effect of temperature on the density and orientation of the water molecules in the layer at the ice-silica interface.

COMPUTATIONAL METHOD

Model Silica Surfaces.

Silica is an extremely common material in nature, and semiconductor industry wafers are generally made from single-crystal silicon: the surfaces of which are covered with native oxide grown in air and water (45). It is also well known that the surface of the silicon oxide film with a thickness of a few nanometers is terminated with silanol groups by hydroxylation (46).

In this study, silica slabs with dimensions of $2.33 \times 2.2 \times 2.2$ nm and two different surfaces were prepared from a quartz system consisting of 300 Si atoms and 600 O atoms. A surface was formed after cutting the initial crystal structure parallel to the (1 0 0) face, and it had dangling bonds of Si atoms. The amorphous slab was prepared using the following procedure with a quartz system (47); detailed information is provided in the Supporting Information. As an initial condition, the quartz slab was packed into the simulation box with periodic boundary conditions in the *x*, *y*, and *z* directions. First, the Nosé–Hoover thermostat, a deterministic algorithm for constant-temperature molecular dynamics simulations, was applied to increase the system temperature from 1 to 5000 K for 200 ps, and the system was equilibrated for 800 ps at constant temperature to obtain a liquid structure. The liquid SiO_2 was then quenched from 5000 to 240 K at a cooling rate of 10^{14} K/s, which is known as a cooling rate sufficient to create an amorphous structure (48). Second, the simulation box was expanded in the *z*-direction, and a vacuum region of 2 nm in the *z*-direction was set above the surface. The boundary condition of the *z*-direction changed from periodic to mirror surface. Third, the system was annealed at 800 K for 1 ns and quenched to 240 K for 1 ns to relieve the surface structure. The simulations to build the amorphous state were performed using the Tersoff potential prepared for the SiO system (49), and the time-step width was 0.1 fs. Finally, silanol groups were created by attaching H or OH atoms to O and Si atoms

with dangling bonds. In the case of the surface with silanol groups, the Tersoff potential was also adapted to H atoms (50, 51). Figure 1 shows configurations of the silanol groups of the original crystalline silica and amorphous silica.

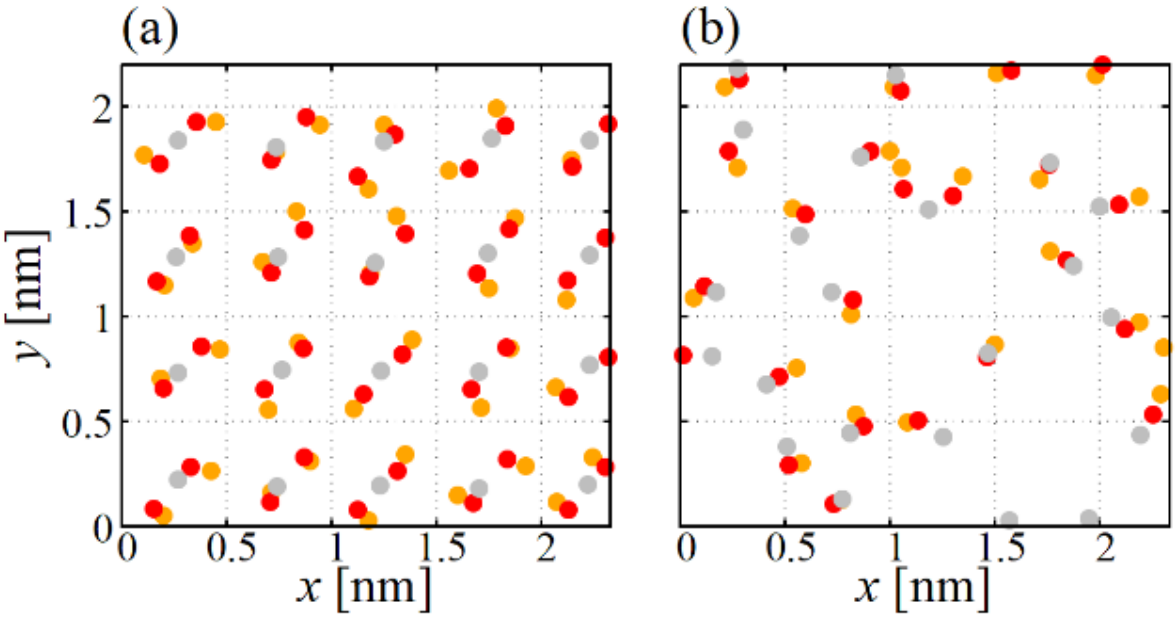

Figure 1. Top view of silicon atoms (gray circle), oxygen atoms (red), and hydrogen atoms (orange) in the silanol group on the silica wall surface for crystalline (a) and amorphous (b).

Water Model.

The water-ice coexistence system was prepared from crystallized ice-block of 2.33 × 2.2 × 7.8 nm size, with 1224 water molecules filling the box imposing periodic boundary condition in the *x*, *y*, and *z* directions. First, the system temperature was controlled at 220 K and 1 atm pressure using a Nosé–Hoover thermostat and barostat for 1 ns. Subsequently, in order to create a liquid region, the simulation box was divided into two slabs in the *z*-direction; each region's temperature was controlled at 300 K on the lower side (wall side) and 1 K on the upper side using the velocity

scaling method for 1 ns. Subsequently, the temperature of the entire system was controlled by the Nosé–Hoover thermostat at 220 K for 1 ns. Here, pressure control was not applied because of the need to fit the ice-water box to the silica slab. The ice region has a hexagonal ice known as I_h structure, and the plane orientation of the ice-water interface is {1120}. The TIP4P/2005 model was adopted for the water molecules because the relationship between the temperature and density around the melting point, agrees well with the experimental values (52).

Simulation Conditions.

The ice-water and silica system described above were combined by positioning copies of the ice-water system normal to the *z*-axis and adjacent to the silica system, as shown in Fig. 2. The overall size of the calculation system was $L_x \times L_y \times L_z = 2.33 \times 2.2 \times 12.3$ nm. The *x* and *y* directions had periodic boundary conditions, and a mirror surface boundary condition was applied to the upper side in the *z*-direction. A vacuum region of approximately 2 nm in the *z*-direction was set above the ice region as the initial condition.

The wall shown in Fig. 2 was used with a fixed layer at the bottom wall with 0.5 nm as width. The Langevin method (53) was applied for temperature control, with a region of 0.5 nm width above the fixed layer used as a phantom layer.

For the interaction between water molecules and the SiO_2 wall, the 12-6 Lennard-Jones (LJ) potential for van der Waals interactions and the Coulomb potential for electrostatic interactions were applied.

$$\phi_{ij}(r_{ij}) = 4\varepsilon_{ij}\left\{\left(\frac{\sigma_{ij}}{r_{ij}}\right)^{12} - \left(\frac{\sigma_{ij}}{r_{ij}}\right)^{6}\right\} + \frac{q_i q_j}{4\pi\varepsilon_0 r_{ij}} \quad (1)$$

where i and j are the numbers of atoms, and r_{ij} is the distance between the two atoms. ε_{ij} and σ_{ij} are the Lennard-Jones parameters, while q_i and q_j are the partial charges of the atoms. The interactions of the LJ parameters between different types of atoms were computed using the Lorentz-Berthelot mixing rules. The velocity Verlet method was used for the numerical integration. The time step integrations for all the systems were performed by the multiple time step integration technique RESPA (54) and the outer time step was set to 2 fs for the LJ potential and the inner time step was set to 0.1 fs for the Tersoff potential. The LAMMPS (55) molecular dynamics simulation software package was used for the calculations.

(a) (b)

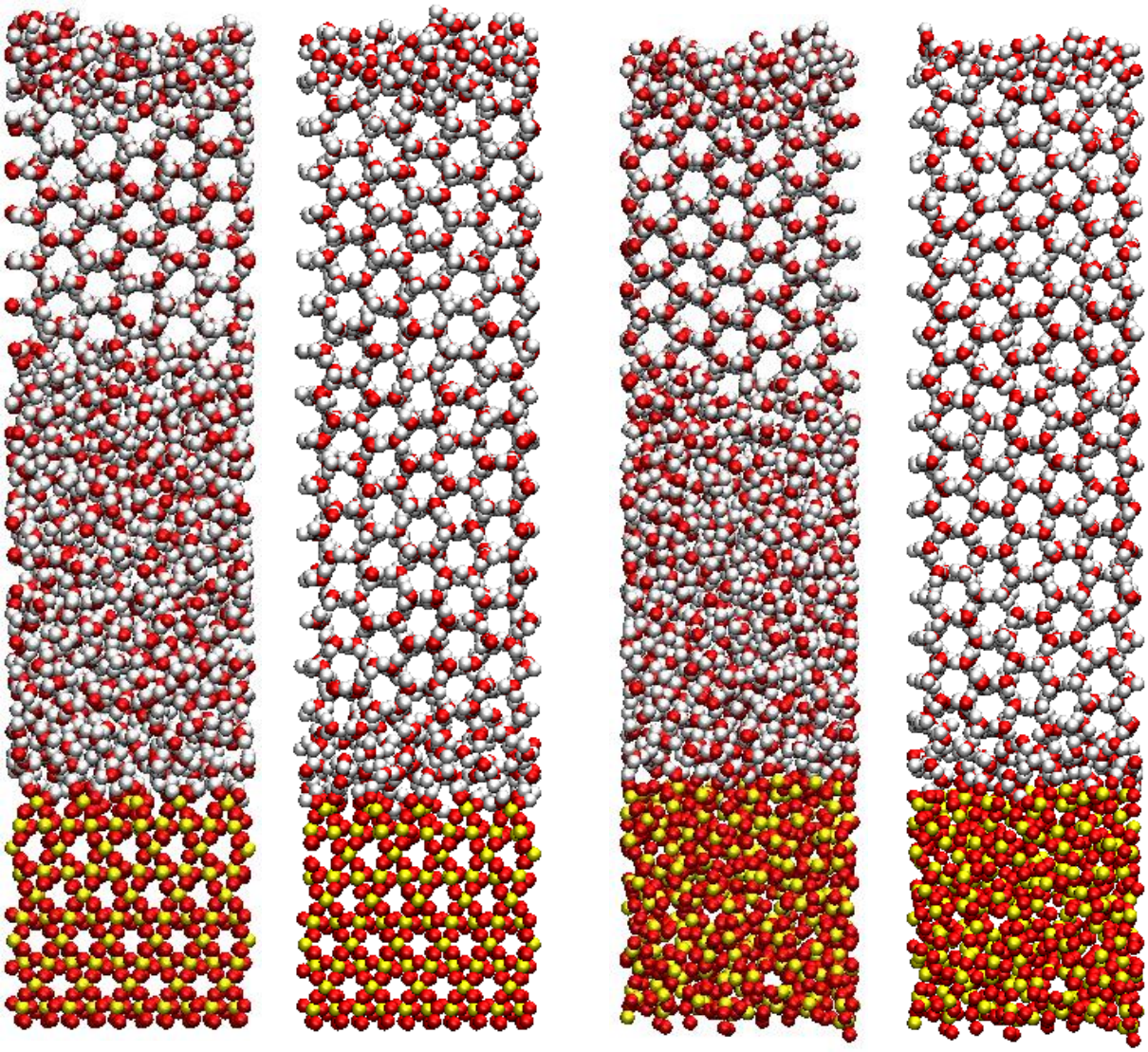

t = 0 ns t = 50 ns t = 0 ns t = 50 ns

Figure 2. Snapshots of the solidification process at t = 0 and 50 ns. (a) Crystalline silica. (b) Amorphous silica.

Simulation Procedure.

The solidification process was simulated using the following procedure. After increasing the temperature of the entire system from 1 K to the target temperature in 1 ns using the Nosé–Hoover method, we ran the simulation without temperature control for 1 ns for relaxation. Subsequently, the temperature of the water molecules in the cooling area (the region above the ice phase: $7 < z < 8$ nm) was controlled using the velocity scaling method as a technique to partially control the temperature of the simulation box. During the entire calculation period, the temperature of the wall phantom layer located above the fixed layer was maintained equivalent to the system temperature using the Langevin method. We determined the melting points of water on the crystalline and amorphous silica models to be 241 K and 244 K, respectively, using the time evaluation of the total energy (Fig. S4 of Supporting Information) (56, 57). Additionally, three system sizes were used to assess the effects of the simulation box size. The solidification process near the wall were performed using the larger simulation cell, which had four and nine times the cross-sectional surface area of the small system shown in Fig. 2 for both crystalline and amorphous silica. And the silanol groups on the amorphous silica surface were randomly configurated in the three calculation systems. At the solidification process in three systems of the simulation box sizes, the density profile and structure of the water molecules near the wall have been confirmed to indicate the consistent trends. And this ensured that the simulation box size and the randomness of the silanol configurations on the amorphous silica did not affect the analysis.

RESULTS AND DISCUSSION

Solidification Process.

First, we discuss the ice solidification on crystalline silica and amorphous silica under the same degree of supercooling with crystalline silica at 238 K and amorphous silica at 241 K as the cooling temperatures. In this study, the degree of supercooling was defined as $T_{\text{degree of supercooling}} = T_{\text{melting point}} - T_{\text{cooling temperature}}$.

. Figure 2 shows the initial configurations and snapshots at t = 50 ns when the ice interface was in contact with the silica surface. Figures 3 (a) and 3 (b) show the time evolution of the minimum position of bulk ice crystals determined by the hydrogen bond (58) lifetime ($t_{\text{life}} \geq 2$ ns) and in this study, the minimum position is defined as the tip of the solidification interface. Here, we adopted three geometrical criteria (59) to distinguish the hydrogen bonds; (i) distance of less than 0.35 nm between donor O atom and acceptor O atom, (ii) distance of less than 0.25 nm between donor H atom and acceptor O atom, and (iii) angle of less than 30° between the direction of donor O–acceptor O vector and the OH-bond vector of the donor.

In Fig. 3 (a) and 3 (b) the gradient of the plot until 30 ns indicates the growth rate of the solidification interface, which is approximately 10 cm/s for both models. Previous computational studies (60) have reported that the growth rate of the ice interface is 10 cm/s under supercooling of 15 K that of the molecular dynamics simulation using the TIP4P/2005 water model without a wall. The ice interface reaches the wall surface at approximately t = 35-40 ns for crystalline silica and at approximately t = 25-35 ns in the case of amorphous silica. After reaching the wall surface the position of the ice interface fluctuates on the wall surface, and it can be seen that the distance between the wall surface and the ice interface is approximately 1 nm in both the cases.

Figure 3 (c) shows the relationship between the thickness of the layer at the ice-silica interface, commonly known as the QLL, and the temperature. Experimental measurements have confirmed that the thickness of the QLL is about 1.0 nm at a supercooling of 10 K, and the temperature dependence of the QLL thickness is estimated to be 0.03 nm/K (16). The results of these simulations are consistent with the experiments on the amorphous silica surface in terms of the layer thickness and temperature dependence. In these simulations the layer thickness is slightly thinner on the amorphous surface; the details are discussed below.

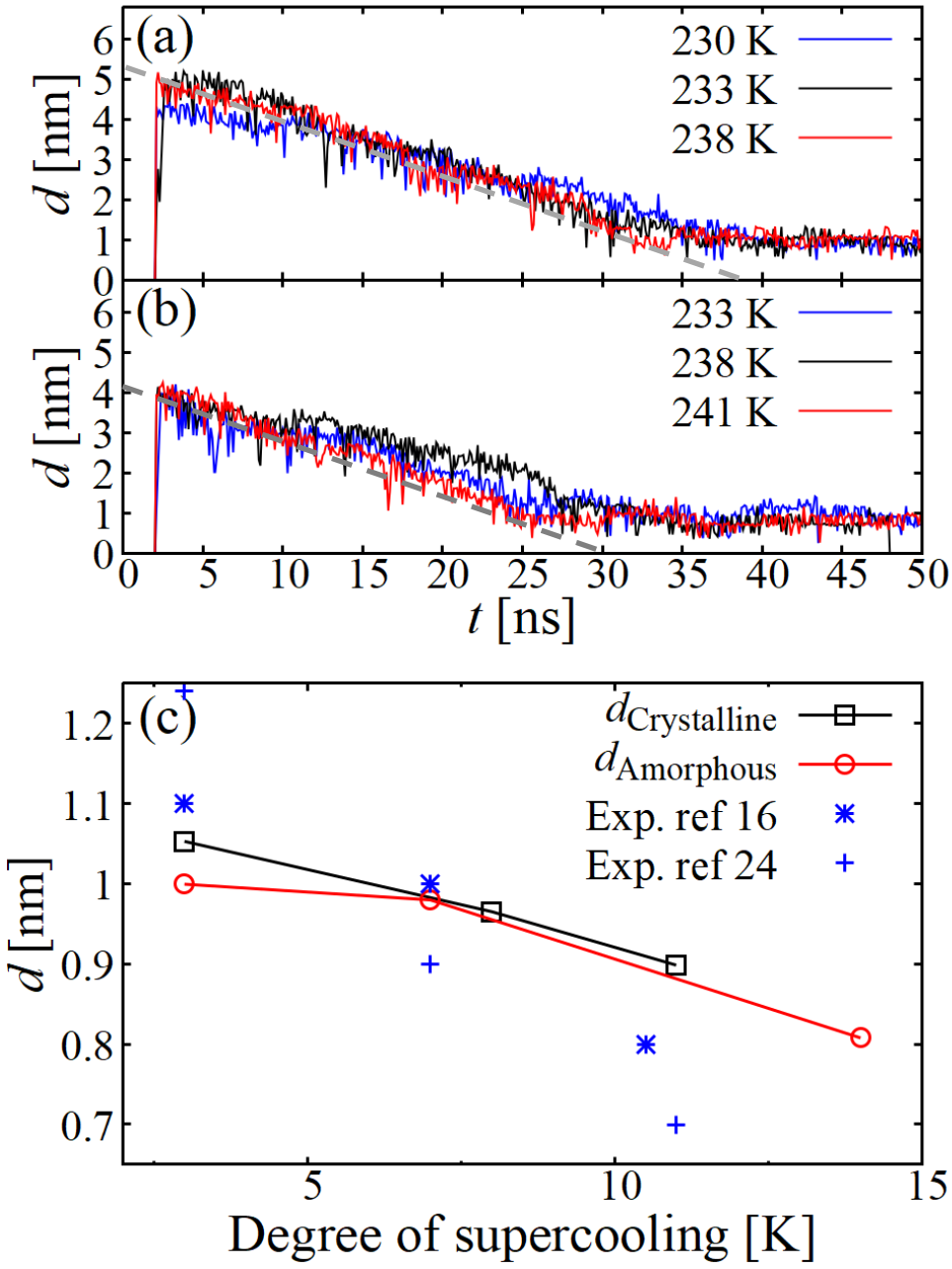

Figure 3. Time evolution of minimum z position of an ice crystal at each temperature; (a) Crystalline silica, and (b) Amorphous silica. (c) indicates the relationship between the layer thickness at ice-silica interface and the degree of supercooling. The thickness was averaged after the solidification interface contacts the wall surface.

Density Profile in the *z*-direction.

To investigate the details of the layer at the ice-silica interface, the density profiles of the silica wall (i.e., Si, O, and H atoms) and water molecules are shown in Fig. 4. These results were obtained for crystalline silica at 238 K and amorphous silica at 241 K. The distribution of water molecules demonstrates liquid water and solid ice states in relation to the z position near the wall surface, which were calculated as the time-average values during 10 ns; the liquid water state was between 0 ns and 10 ns, the solid ice state was between 40 and 50 ns, and were computed for each condition by averaging the histogram of densities along z over the set of 1000 configurations.

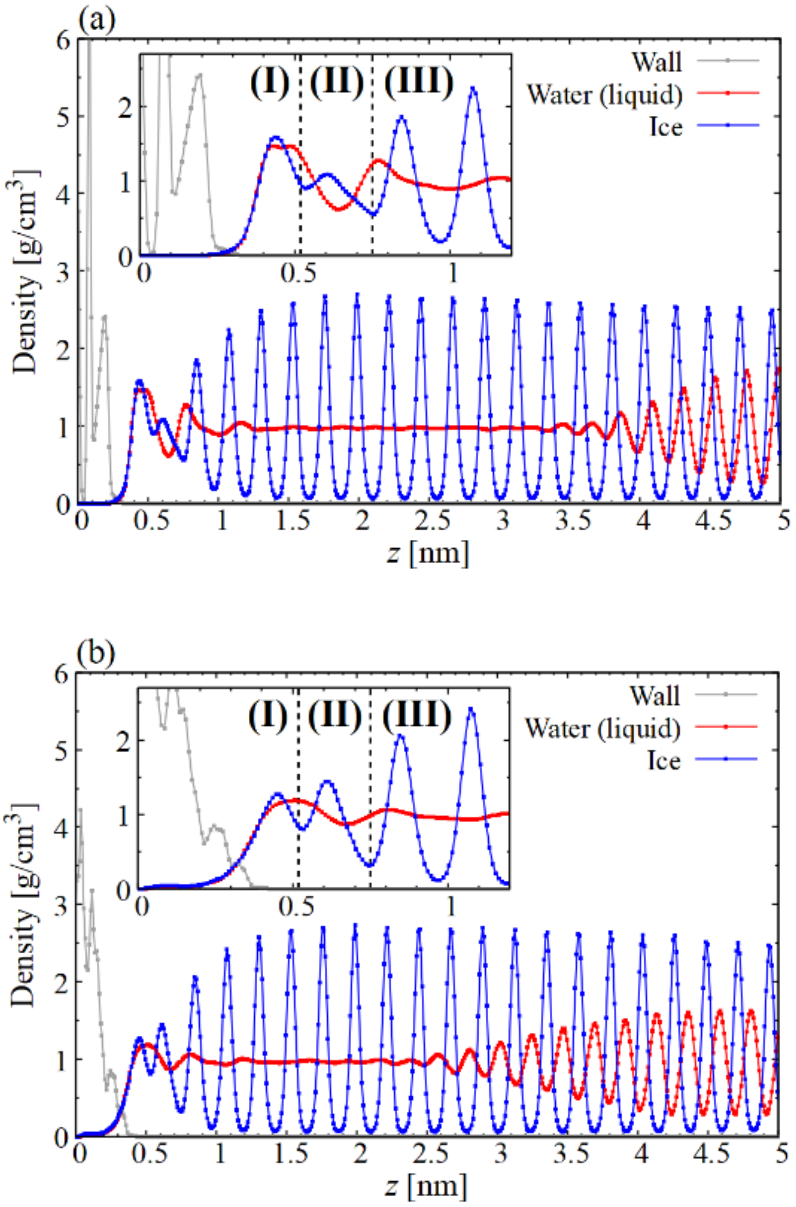

Figure 4. Density profile of silica walls (gray plot) and water molecules in the z-direction. The distribution of water molecules is in the liquid water state (red plot) and the solid ice state (blue plot) for the crystalline silica (a) and amorphous silica (b). The close up panels show the region in the vicinity of the wall surface, where the regions are defined; (I) $0 < z < 0.52$ nm, (II) $0.52 < z < 0.75$ nm, and (III) $z > 0.75$ nm.

In Fig. 4 (a) and 4 (b), the first density peak near the silica wall is affected by the silanol groups, especially in the liquid state (red line), and the peak in the case of the crystalline silica is higher than that in the case of the amorphous silica. The intensity of the density peak of the adsorption layer correlates with the density of the silanol groups, and crystalline silica has a larger density peak of the adsorption layer.

Focusing on the ice state, the region of the ice bulk area shows periodic peaks because the water molecules are structured in the form of ice crystals. The intensity of the density peak gradually decreases in the vicinity of the wall surface. This implies that the ice interface is not permanently maintained and fluctuates in this area.

In the region at $z < 0.75$ nm, two density peaks of the adsorption layer appear after the ice interface contacts the silica surface. The density bilayer was confirmed on the ice surface in contact with air and water molecules were disordered in the bilayer (29): Fig. 4 shows that the bilayer appears in the layer at the ice-silica interface. To investigate the details of this bilayer surface, we have divided the z-direction region into (I) the area of the first density peak, (II) the area of the second density peak, and (III) the bulk area, and have discussed the density distribution, orientations of water molecules in each region, and the effect of temperature on them in the following section.

Density and Structure of Water Molecules in Bulk Area.

Figure 5 shows the two-dimensional density distribution of the bulk region ($1.5 < z < 2.0$ nm) in the *xy* plane parallel to the wall surface. The profiles are the average values for the duration of 1 ns, and water (liquid) and ice (solid) states are the data at $t = 1$ ns and $t = 50$ ns, respectively. The density distribution is uneven in the water (liquid) state shown in Fig. 5 (a), which is presumed to be due to the supercooled state before solidification. Similar to the *z*-direction distribution, the water density distribution becomes periodic as the area solidifies, and there is almost no difference in the distribution tendency between crystalline and amorphous silica cases.

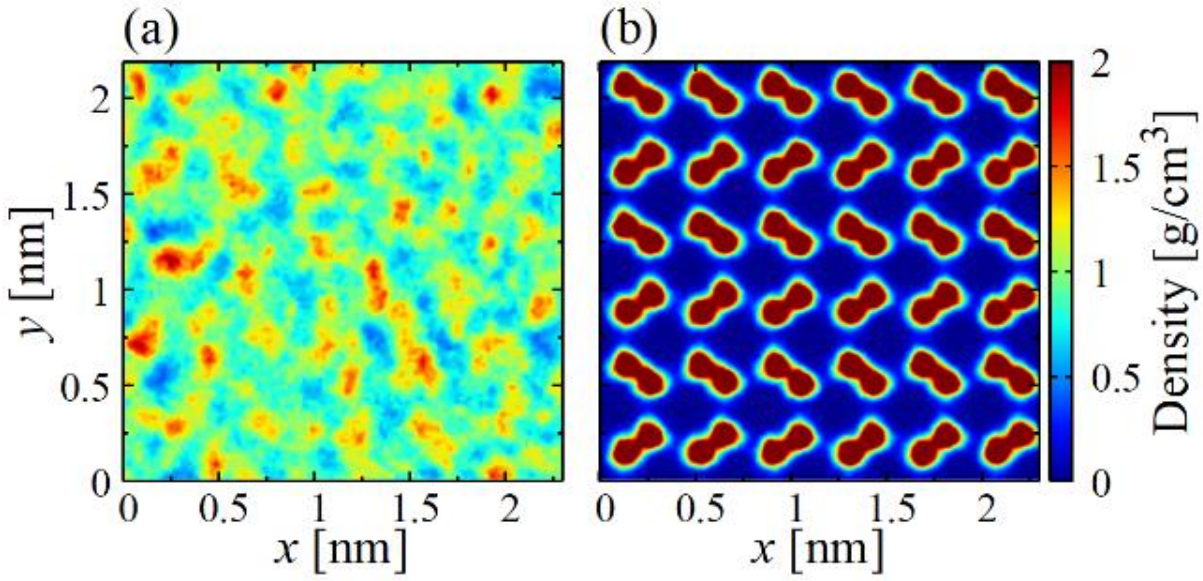

Figure 5. Two-dimensional density maps of water molecules in the area of $1.5 < z < 2.0$ nm on the amorphous silica; (a) liquid state at $t = 1$ ns, and (b) ice state at $t = 50$ ns.

To investigate the structure of water, adjacent to the silica surface, we parameterized the orientation of water molecules in terms of Euler angles to the *z*-axis as illustrated in Fig. 6 (a). The polar angle of a molecule is defined using each vector; the dipole angle is between the water symmetry axis and *z*-direction, and the OH angle is between the OH vector and *z*-direction (61). Figures 6 (b) and 6 (c) show the two-dimensional angular probability (*P*) map of water molecules in the bulk region ($1.5 < z < 2.0$ nm), and Fig. 7 (d) illustrates the typical orientation of water molecules in the map. The distribution map of the ice state indicates that water molecules have six orientations in the ice crystal. In addition, in the angular distributions shown in Fig. 6 (b) and 6 (c), the ratios of the six orientations that form the ice crystals are shown in Fig. 6 (e). This result indicates that the ice crystals contain a similar proportion of the six orientations.

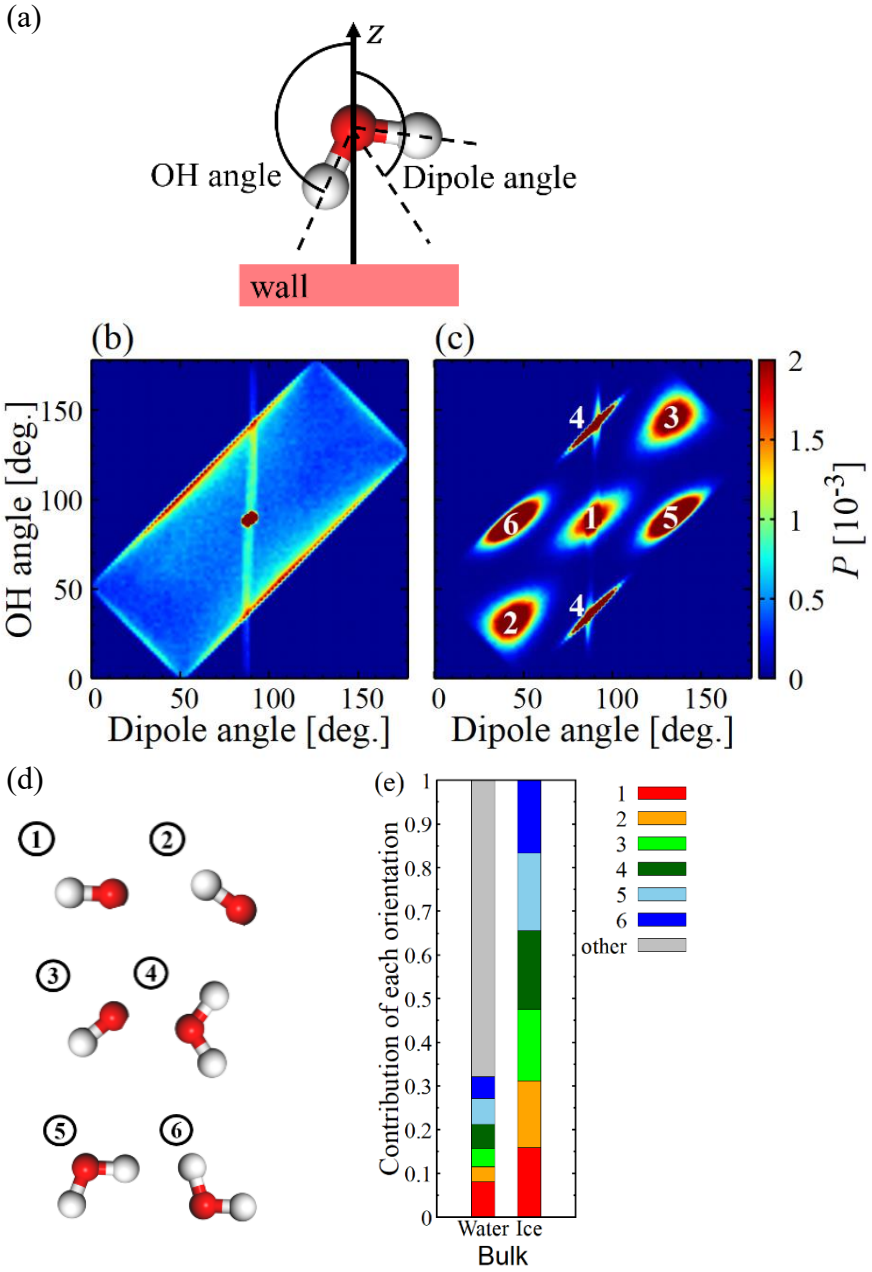

Figure 6. (a) Schematic drawing of OH bond and dipole vector angles. Two-dimensional angular probability mappings of (b) liquid state, (c) ice state of water molecules in the bulk region ($1.5 < z < 2.0$ nm). (d) Six main orientations of water molecules in the bulk ice crystals and the numbers in (c) represent the corresponding areas in the two-dimensional angular probability mapping. (e) Ratio of orientations in the angular probability map.

Density and Structure of Water Molecules near the Wall.

To investigate the density map of water molecules near the wall area, i.e., (I) first peak and (II) second peak as defined in Fig. 4, the density maps of the *xy* plane are shown in Fig. 7 for areas (I) and (II). The distributions of the density maps of area (I) shown in Fig. 7(a)-7(d) correspond to the position of silanol groups in Fig. 1, and it indicates an abundance of water molecules between the silanol groups. It is known that this configuration of water molecules bridges different silanol groups by forming hydrogen bonds, which lowers the adsorption energy (62). On the contrary, the density map of area (II) does not have a characteristic distribution, indicating that the water molecules in this region are not affected by the silanol groups. In the ice state, density maps in Fig. 7 (f) and 7 (h) show that water molecules are unevenly distributed on both the silica wall surfaces, and this tendency was more remarkable on the amorphous wall surface. This uneven density distribution is due to ice crystallization, indicating that the water molecules in area (II) were more affected by the ice interface than the silanol groups.

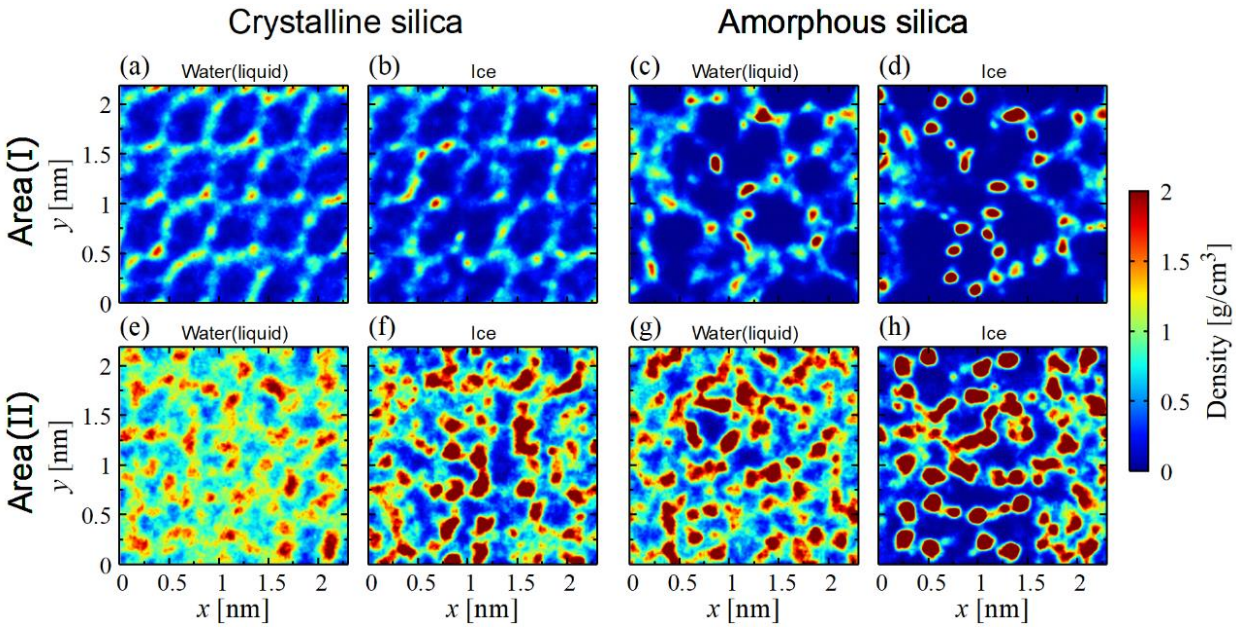

Figure 7. Density maps of water molecules, (a)-(d) in the area (I) and (e)-(h) in the area (II). Areas (I) and (II) represent the density of water molecules present in the $0 < z < 0.52$ nm and $0.52 < z < 0.75$ nm regions, respectively.

Figure 8 shows the angular probability ratio of each region before and after the ice interface reached the silica wall surface. In both crystalline and amorphous cases in area (I), the orientation of State No. 1 in Fig. 6 (d) increases compared to the bulk liquid state. The increase in State No. 1 near the wall surface is remarkable on the crystalline silica surface owing to the increase of hydrogen bonds between water and silanol groups; this indicates that the higher the silanol group density on the surface, the stronger the directionality of the water orientation. These trends of the water orientation are consistent with previous experimental (23) and computational (63) studies.

In region (II), the angular distributions in the liquid state are not significantly different from the bulk region because of the weaker interactions with the silanol groups.

After the ice surface approached the wall surface, the total ratio of the six orientations increased in area (II), which implies that the water molecules tend to have an ice structure. From Fig. 3 (a) and 3 (b) it is evident that ice crystals are not permanently maintained in this region; however, the ratio increment of the six orientations implies that the approach of the ice interface led to temporary ice crystal formation. Furthermore, Fig. 8 shows that the ratio increments caused by ice crystallization contributed to the increase in State No. 2–6 orientation. This ratio increment is related to the intensity of the density peak in Fig. 4, and a stronger density peak appears on the amorphous wall surface where the orientation change is remarkable.

In contrast, State No. 2–6 orientation increases slightly in area (I), indicating that area (I) is less susceptible to the approach of the ice interface and the frequency of the temporal ice crystallization is low. This result suggests that the water molecules in this region have a structure which is different from an ice structure.

When comparing crystalline and amorphous silica in the ice state, the total ratio of State No. 2–6 orientation of water molecules is higher on the amorphous surface in both areas (I) and (II). This indicates that water molecules on the amorphous silica surface are more likely to crystallize than those on the crystalline silica surface, which is consistent with Fig. 3 (c) where the thickness of the layer at the ice-silica interface is thinner on the amorphous surface.

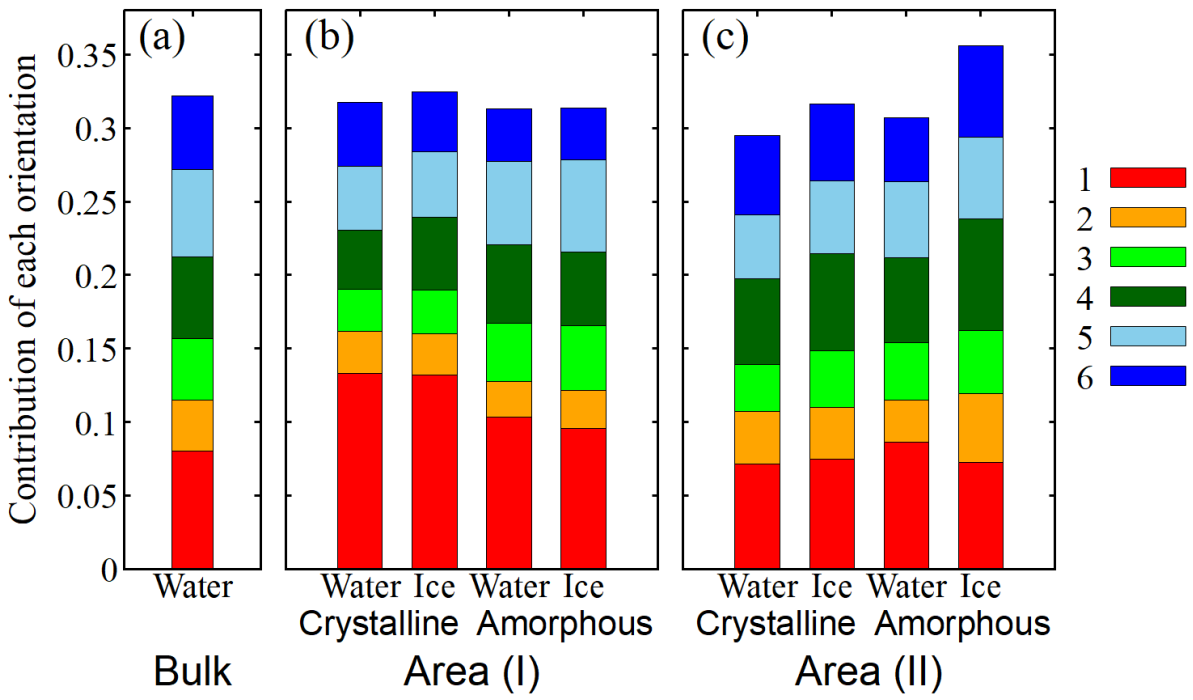

Figure 8. Angular probability ratio of water molecules in (a) bulk, (b) area (I) and (c) area (II). Areas (I) and (II) represent the density of water molecules present in the $0 < z < 0.52$ nm and $0.52 < z < 0.75$ nm regions, respectively. State No. 1-6 show the orientation of the water molecules illustrated in Fig. 6 (d).

Effects of Temperature on the Layer at Ice-silica Interface.

Figure 9 shows the ratio of the orientations of water molecules in areas (I) and (II) when the cooling temperature is changed on each of the crystalline (238 K, 233 K, and 230 K) and amorphous (241 K, 238 K, and 230 K) silica walls.

In area (II), the ice crystallization progresses on the crystalline and amorphous silica surfaces according to the low temperature level and crystallization occurs more frequently on the amorphous silica surface. This tendency is consistent with the relationship between the

temperature and thickness of the layer at the ice-silica interface as shown in Fig. 3 (c). In contrast, such a characteristic temperature dependent behavior could not be observed in area (I).

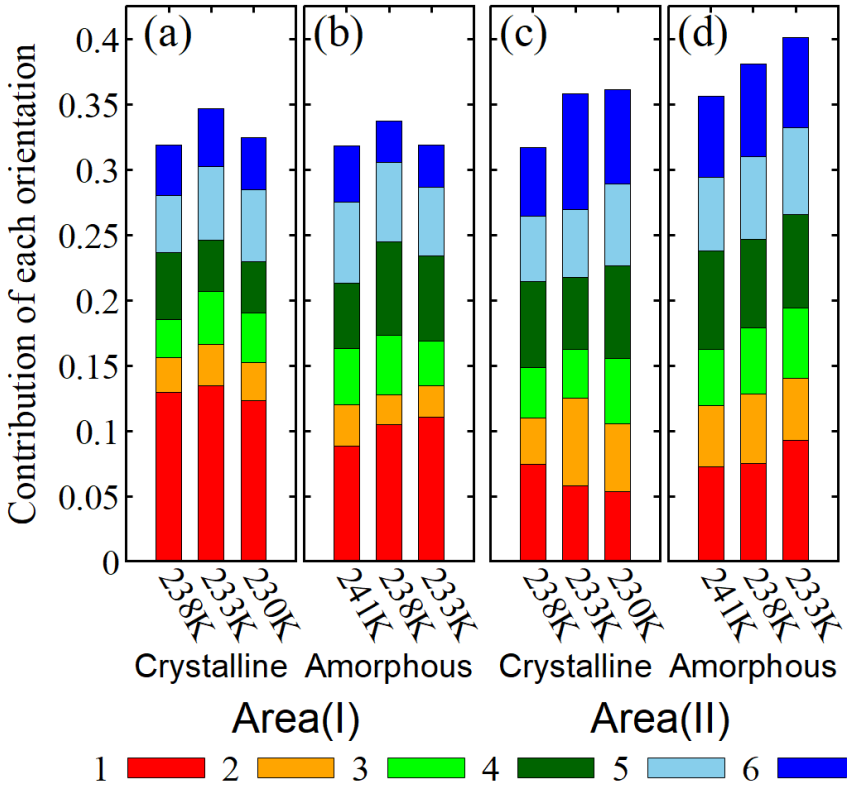

Figure 9. The degree of crystallization in area (I) and (II) at each degree of supercooling on crystalline and amorphous silica.

To interpret the change in orientation affected by the temperature, the difference in angular probability distribution before and after the solidification, the *z*-direction distribution of the density, and the potential energy are shown in Fig. 10. The difference maps were calculated using angular probability (P) as $P_{\mathrm{Difference}} = P_{\mathrm{Ice}} - P_{\mathrm{Water(liquid)}}$, and the potential energy ($E_{\mathrm{potential}}$) is computed as the per-atom potential energy for each atom. In the region of the ice crystals, periodicity appears in the *z*-direction profile as ice crystallizes and the potential energy becomes lower in the high-density region.

In area (II), the intensity of the density peak increases with decreasing temperature on the crystalline silica surface, as shown in Fig. 10 (i). This behavior agrees well with the crystallinity of water molecules (total value of the contribution of each orientation) on the crystalline silica surface shown in Fig. 9 (c). On the other hand, the crystallinity of the water molecules increases with decreasing temperature on the amorphous surface shown in Fig. 9 (d), as in the case of the crystalline silica surface. However, the peak intensities of area (II) in the density profiles shown in Fig. 10 (iii) do not change with temperature, and it implies that the area (II) of the amorphous silica surface is sufficiently ice-crystallized compared to that of the crystalline silica surface at the same supercooling degree of 3 K (crystalline:238 K and amorphous:240 K). Furthermore, the difference maps of the angular probability indicate that the orientation has changed from State No. 1 to No. 2–6 as shown in Fig. 6 (d). The lower the temperature, the stronger the orientation shifts, suggesting that this is due to ice crystallization. Regarding the result of area (II), the orientation shift in the difference map seems to be consistent with the orientation ratio in Fig. 9, which means that the water molecules in area (II) have an ice structure.

In area (I), the profiles of density and potential energy are unlikely to change with temperature, matching the orientation ratio pattern in Fig. 9. In contrast, the difference maps of the angle distribution show a remarkable change corresponding to the temperature, indicating that the number of water molecules with State No. 1 consistently decreases and water molecules with the orientation around State No. 1 increase. The sites of increased orientations are slightly shifted from the orientation sites of State No. 2–6 indicating that the water molecules in this area have a different orientation than that of the ice crystals. Such a structure is considered to be the ice-like structure and the orientation ratio in Fig. 9 did not show temperature dependence because the water molecules had orientation sites except for the site defined in Fig. 6. However, the difference maps

show that orientations are unevenly distributed depending on the temperature, and it was found that the water molecules in area (I) were also affected by temperature. Ice crystallization in area (I) could not be confirmed in the temperature range of these simulations; however it is revealed that the water molecules have an ice-like structure and temperature dependence.

Studies in the past have documented that water molecules in the bilayer region of the density profile solidify at lower temperatures (64). It implies that the structure of the water molecules in area (I) may change from the ice-like to the ice structure depending on the temperature. The structure of the layer at the ice-silica interface needs further investigation.

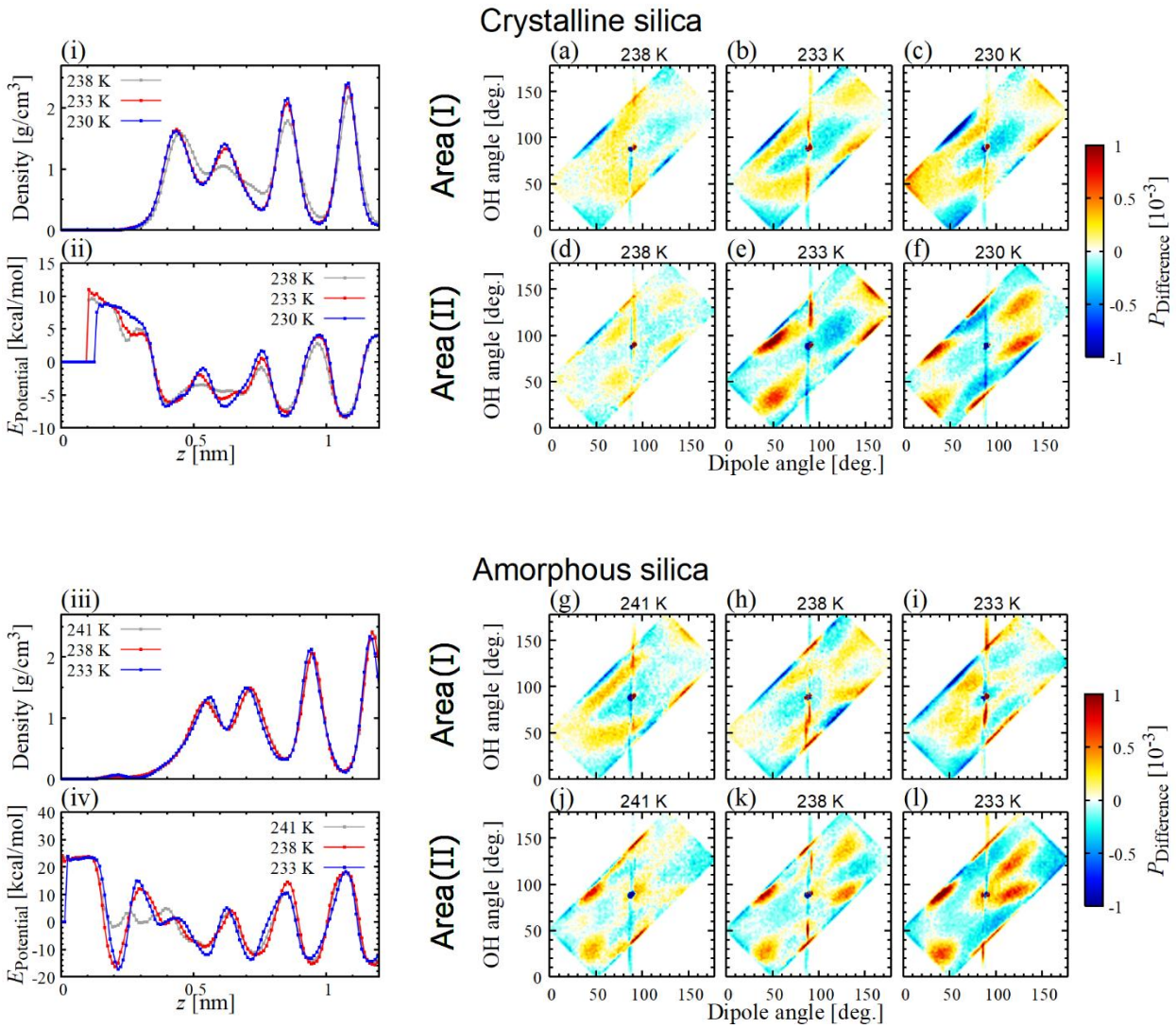

Figure 10. (i)-(iv) *z*-direction distribution of density and the per-atom potential energy for each atom at each controlled temperature. (a)-(l) the difference of angular probability before and after the solidification interface contacts to the wall surface.

CONCLUSION

We examined the structure of water molecules at the ice-silica interface on two types of silica surfaces at various temperatures and calculated the density and molecular orientations using molecular dynamics simulations. The results showed that the water molecules near the wall surface have a density distribution and an orientation influenced by the silanol groups in the water (liquid) and ice (solid) states; the effect was evident particularly on crystalline silica with high silanol group density. In the layer at the ice-silica interface, water molecules undergo temporary crystallization and melting and permanent ice crystallization does not occur. The thickness of this non-freezing layer is consistent with the experimental QLL thickness and temperature dependence. Two density peaks appeared in the layer, and the intensities of the peaks and their profiles were affected by the density of the silanol groups and the degree of supercooling.

Water molecules crystalize and melt repeatedly in the bilayer and this temporary ice crystallization occurs more frequently on the ice interface side of the density bilayer and on the amorphous silica surface. The density and orientation distribution of water molecules revealed that the density of the silanol groups on the wall surface and the distance from the silanol groups affected ice crystallization. It was also confirmed that lower the temperature, the more ice crystallization progressed in the layer and the tendency was remarkable on the amorphous wall surface. Furthermore, it was clarified that the structure of the bilayer on the ice interface side was the same as that of ice crystals and that the wall surface side had a structure close to that of ice crystals.

Our simulations would contribute to further the understanding of the layer properties at the ice-silica interface and interpret the interaction between the state of wall surface and the solidification phenomena in the vicinity of the wall. Studies in the past have documented that the surface

crystallizes completely at the vapor–ice interface at a deeper degree of supercooling (64) and verification is also necessary at the ice-substrate interface.

AUTHOR INFORMATION

Supporting Information

System preparation for amorphous silica wall and confirmation of melting point.

Corresponding Author

1. Full name: Shota Uchida

Email address: sh.uchidaascreen.co.jp

Institutional affiliation: Osaka University, SCREEN Holdings Co., Ltd.,

Mailing address: 322 Furukawa-cho, Hazukashi, Fushimi-ku, Kyoto, Kyoto 612-8486, Japan

2. Full name: Kunio Fujiwara

Email address: k.fujiwara@mech.eng.osaka-u.ac.jp

Institutional affiliation: Osaka University, Japan Science and Technology Agency

Mailing address: 2-1 Yamadaoka, Suita, Osaka 565-0871, Japan

3. Full name: Masahiko Shibahara

Email address: siba@mech.eng.osaka-u.ac.jp

Institutional affiliation: Osaka University

Mailing address: 2-1 Yamadaoka, Suita, Osaka 565-0871, Japan

Author Contributions

The manuscript was written through contributions of all authors. All authors have given approval to the final version of the manuscript.

REFERENCES

1. Li, Y.; Somorjai, G. A. Surface Premelting of Ice. *J. Phys. Chem. C* **2007**, *111* (27), 9631–9637.

2. Dash, J. G.; Rempel, A. W.; Wettlaufer, J. S. The Physics of Premelted Ice and Its Geophysical Consequences. *Rev. Mod. Phys.* **2006**, *78* (3), 695–741.

3. Rosenberg, R. Why Is Ice Slippery? *Phys. Today* **2005**, *58* (12), 50–54.

4. Emelyanenko, K. A.; Emelyanenko, A. M.; Boinovich, L. B. Water and Ice Adhesion to Solid Surfaces: Common and Specific, the Impact of Temperature and Surface Wettability. *Coatings* **2020**, *10* (7), 1–23.

5. Bartels-Rausch, T. Ten Things We Need to Know about Ice and Snow. *Nature* **2013**, *494* (7435), 27–29.

6. Fujiwara, K.; Sasaki, S.; Shibahara, M. A Molecular Dynamics Study on Effects of Solidification Phenomena on Water Molecules in the Vicinity of a Solid Surface. *Therm. Sci. Eng.* **2016**, *25* (4), 9–16.

7. Fujiwara, K.; Shibahara, M. A Molecular Dynamics Study on Wetting Phenomena at a Solid Surface with a Nanometer-Scale Slit Pore. *Nano. Micro. Therm. Eng.* **2013**, *17* (1), 1–9.

8. An, J.; Lee, H.; Kim, H.; Jeong, H. Effect of Process Parameters on Particle Removal Efficiency in Poly(Vinyl Alcohol) Brush Scrubber Cleaning. *Jpn. J. Appl. Phys.* **2012**, *51* (2 part 1).

9. Uchida, S.; Fujiwara, K.; Shibahara, M. Molecular Dynamics Study of Interactions between the Water/Ice Interface and a Nanoparticle in the Vicinity of a Solid Surface. *Nanoscale Microscale Thermophys. Eng.* **2020**, *24* (2), 53–65.

10. Nagata, Y.; Hama, T.; Backus, E. H. G.; Mezger, M.; Bonn, D.; Bonn, M.; Sazaki, G. The Surface of Ice under Equilibrium and Nonequilibrium Conditions. *Acc. Chem. Res.* **2019**, *52* (4), 1006–1015.

11. Bartels-Rausch, T.; Jacobi, H. -W.; Kahan, T. F.; Thomas, J. L.; Thomson, E. S.; Abbatt, J. P. D.; Ammann, M.; Blackford, J. R.; Bluhm, H.; Boxe, C.; Domine, F.; Frey, M. M.; Gladich, I.; Guzmán, M. I.; Heger, D.; Huthwelker, T.; Klán, P.; Kuhs, W. F.; Kuo, M. H.; Maus, S.; Moussa, S. G.; McNeill, V. F.; Newberg, J. T.; Pettersson, J. B. C.; Roeselová, M.; Sodeau, J. R. A Review of Air-Ice Chemical and Physical Interactions (AICI): Liquids, Quasi-Liquids, and Solids in Snow. *Atmos. Chem. Phys.* **2014**, *14* (3), 1587–1633.

12. Furukawa, Y.; Ishikawa, I. Direct Evidence for Melting Transition at Interface between Ice Crystal and Glass Substrate. *J. Cryst. Growth* **1993**, *128* (1–4 part 2), 1137–1142.

13. Morishige, K.; Nobuoka, K. X-Ray Diffraction Studies of Freezing and Melting of Water Confined in a Mesoporous Adsorbent (MCM-41). *J. Chem. Phys.* **1997**, *107* (17), 6965–6969.

14. Morishige, K. Influence of Pore Wall Hydrophobicity on Freezing and Melting of Confined Water. *J. Phys. Chem. C* **2018**, *122* (9), 5013–5019.

15. Li, H.; Bier, M.; Mars, J.; Weiss, H.; Dippel, A. C.; Gutowski, O.; Honkimäki, V.; Mezger, M. Interfacial Premelting of Ice in Nano Composite Materials. *Phys. Chem. Chem. Phys.* **2019**, *21* (7), 3734–3741.

16. Engemann, S.; Reichert, H.; Dosch, H.; Bilgram, J.; Honkimäki, V.; Snigirev, A. Interfacial Melting of Ice in Contact with SiO2. *Phys. Rev. Lett.* **2004**, *92* (20), 205701.

17. Butt, H. J.; Döppenschmidt, A.; Hüttl, G.; Müller, E.; Vinogradova, O. I. Analysis of Plastic Deformation in Atomic Force Microscopy: Application to Ice. *J. Chem. Phys.* **2000**, *113* (3), 1194–1203.

18. Pittenger, B.; Fain, S. C.; Cochran, M. J.; Donev, J. M. K.; Robertson, B. E.; Szuchmacher, A.; Overney, R. M. Premelting at Ice-Solid Interfaces Studied via Velocity-Dependent Indentation with Force Microscope Tips. *Phys. Rev. B* **2001**, *63* (13), 1–15.

19. Algara-Siller, G.; Lehtinen, O.; Wang, F. C.; Nair, R. R.; Kaiser, U.; Wu, H. A.; Geim, A. K.; Grigorieva, I. V. Square Ice in Graphene Nanocapillaries. *Nature* **2015**, *519* (7544), 443–445.

20. Yuk, J. M.; Park, J.; Ercius, P.; Kim, K.; Hellebusch, D. J.; Crommie, M. F.; Lee, J. Y.; Zettl, A.; Alivisatos, A. P. High-Resolution EM of Colloidal Nanocrystal Growth Using Graphene Liquid Cells. *Science* **2012**, *336* (6077), 61–64.

21. Sazaki, G.; Asakawa, H.; Nagashima, K.; Nakatsubo, S.; Furukawa, Y. How Do Quasi-Liquid Layers Emerge from Ice Crystal Surfaces? *Cryst. Growth Des.* **2013**, *13* (4), 1761–1766.

22. Endo, A.; Yamamoto, T.; Inagi, Y.; Iwakabe, K.; Ohmori, T. Characterization of Nonfreezable Pore Water in Mesoporous Silica by Thermoporometry. *J. Phys. Chem. C* **2008**, *112* (24), 9034–9039.

23. Anderson, A.; Ashurst, W. R. Interfacial Water Structure on a Highly Hydroxylated Silica Film. *Langmuir* **2009**, *25* (19), 11549–11554.

24. Liljeblad, J. F. D.; Furó, I.; Tyrode, E. C. The Premolten Layer of Ice next to a Hydrophilic Solid Surface: Correlating Adhesion with Molecular Properties. *Phys. Chem. Chem. Phys.* **2016**, *19* (1), 305–317.

25. Abe, J.; Hirano, N.; Tsuchiya, N. Infrared Spectroscopic Study of Water in Mesoporous Silica under Supercritical Conditions. *J. Mater. Sci.* **2012**, *47* (23), 7971–7977.

26. Huang, Y. R.; Liu, K. H.; Mou, C. Y.; Sun, C. K. Relaxation Dynamics of Surface-Adsorbed Water Molecules in Nanoporous Silica Probed by Terahertz Spectroscopy. *Appl. Phys. Lett.* **2015**, *107* (8).

27. Hayward, J. A.; Haymet, A. D. J. The Ice/Water Interface: Molecular Dynamics Simulations of the Basal, Prism, {20$\bar{2}$1}, and {21$\bar{1}$0} Interfaces of Ice Ih. *J. Chem. Phys.* **2001**, *114* (8), 3713–3726.

28. Nada, H.; Furukawa, Y. Anisotropy in Growth Kinetics at Interfaces between Proton-Disordered Hexagonal Ice and Water: A Molecular Dynamics Study Using the Six-Site Model of H2O. *J. Cryst. Growth* **2005**, *283* (1–2), 242–256.

29. Kling, T.; Kling, F.; Donadio, D. Structure and Dynamics of the Quasi-Liquid Layer at the Surface of Ice from Molecular Simulations. *J. Phys. Chem. C* **2018**, *122* (43), 24780–24787.

30. Zhang, X. X.; Lü, Y. J.; Chen, M. Crystallisation of Ice in Charged Pt Nanochannel. *Mol. Phys.* **2013**, *111* (24), 3808–3814.

31. Moore, E. B.; De La Llave, E.; Welke, K.; Scherlis, D. A.; Molinero, V. Freezing, Melting and Structure of Ice in a Hydrophilic Nanopore. *Phys. Chem. Chem. Phys.* **2010**, *12* (16), 4124–4134.

32. Nouri-Khorasani, A.; Malek, K.; Eikerling, M. Molecular Modeling of Hydronium Ion and Water Distribution in Water-Filled Pt Nanochannels with Corrugated Walls. *Electrocatalysis* **2014**, *5* (2), 167–176.

33. Zhang, X. X.; Chen, M.; Fu, M. Impact of Surface Nanostructure on Ice Nucleation. *J. Chem. Phys.* **2014**, *141* (12), 124709.

34. Naruke, Y.; Kosaka, S.; Nakano, T.; Kikugawa, G.; Ohara, T. A Molecular Dynamics Study on Mass Transport Characteristics in the Vicinity of SiO 2 -Water/IPA Interfaces. *Int. J. Heat Mass Transf.* **2015**, *84*, 584–591.

35. Yang, J.; Meng, S.; Xu, L. F.; Wang, E. G. Ice Tessellation on a Hydroxylated Silica Surface. *Phys. Rev. Lett.* **2004**, *92* (14), 146102.

36. Giovambattista, N.; Rossky, P. J.; Debenedetti, P. G. Effect of Temperature on the Structure and Phase Behavior of Water Confined by Hydrophobic, Hydrophilic, and Heterogeneous Surfaces. *J. Phys. Chem. B* **2009**, *113* (42), 13723–13734.

37. Hassanali, A. A.; Singer, S. J. Model for the Water - Amorphous Silica Interface: The Undissociated Surface. *J. Phys. Chem. B* **2007**, *111* (38), 11181–11193.

38. Katasho, Y.; Liang, Y.; Murata, S.; Fukunaka, Y.; Matsuoka, T.; Takahashi, S. Mechanisms for Enhanced Hydrophobicity by Atomic-Scale Roughness. *Sci. Rep.* **2015**, *5*, 1–12.

39. Chai, J.; Liu, S.; Yang, X. Molecular Dynamics Simulation of Wetting on Modified Amorphous Silica Surface. *Appl. Surf. Sci.* **2009**, *255* (22), 9078–9084.

40. Furukawa, S. I.; Nishiumi, T.; Aoyama, N.; Nitta, T.; Nakano, M. A Molecular Simulation Study on Adsorption of Acetone/Water in Mesoporous Silicas Modified by Pore Surface Silylation. *J. Chem. Eng. Japan* **2005**, *38* (12), 999–1007.

41. Chiricotto, M.; Martelli, F.; Giunta, G.; Carbone, P. Role of Long-Range Electrostatic Interactions and Local Topology of the Hydrogen Bond Network in the Wettability of Fully and Partially Wetted Single and Multilayer Graphene. *J. Phys. Chem*. C **2021**, 125 (11), 6367–6377.

42. Martelli, F.; Crain, J.; Franzese, G. Network Topology in Water Nanoconfined between Phospholipid Membranes. *ACS Nano* **2020**, 14 (7), 8616–8623.

43. Bonnaud, P. A.; Coasne, B.; Pellenq, R. J. M. Molecular Simulation of Water Confined in Nanoporous Silica. *J. Phys. Condens. Matter* **2010**, 22 (28), 1–15.

44. Melnikov, S. M.; Höltzel, A.; Seidel-Morgenstern, A.; Tallarek, U. Adsorption of Water–Acetonitrile Mixtures to Model Silica Surfaces. *J. Phys. Chem. C* **2013**, 117 (13), 6620–6631.

45. Morita, M.; Ohmi, T.; Hasegawa, E.; Kawakami, M.; Ohwada, M. Growth of Native Oxide on a Silicon Surface. *J. Appl. Phys.* **1990**, *68* (3), 1272–1281.

46. Zhuravlev, L. T. The Surface Chemistry of Amorphous Silica. Zhuravlev Model. *Colloids Surf. A Physicochem. Eng. Asp.* **2000**, *173* (1–3), 1–38.

47. Wang, J.; Rajendran, A. M.; Dongare, A. M. Atomic Scale Modeling of Shock Response of Fused Silica and α-Quartz. *J. Mater. Sci.* **2015**, *50* (24), 8128–8141.

48. Vollmayr, K.; Kob, W.; Binder, K. Cooling-Rate Effects in Amorphous Silica: A Computer-Simulation Study. *Phys. Rev. B Condens. Matter* **1996**, *54* (22), 15808–15827.

49. Munetoh, S.; Motooka, T.; Moriguchi, K.; Shintani, A. Interatomic Potential for Si-O Systems Using Tersoff Parameterization. *Comput. Mater. Sci.* **2007**, *39* (2), 334–339.

50. De Brito Mota, F.; Justo, J. F.; Fazzio, A. Hydrogen Role on the Properties of Amorphous Silicon Nitride. *J. Appl. Phys.* **1999**, *86* (4), 1843–1847.

51. Martinez-Gonzalez, J. A.; English, N. J.; Gowen, A. A. Understanding the Interface between Silicon-Based Materials and Water: Molecular Dynamics Exploration of Infrared Spectra. *A.I.P. Adv.* **2017**, *7* (11).

52. Abascal, J. L.; Vega, C. A General Purpose Model for the Condensed Phases of Water: TIP4P/2005. *J. Chem. Phys.* **2005**, *123* (23), 234505.

53. Schneider, T.; Stoll, E. Molecular Dynamics Study of a Three-Dimensional One-Component Model for Distortive Phase Transitions. *Phys. Rev. B* **1978**, *17* (3), 1302–1322.

54. Tuckerman, M.; Berne, B. J.; Martyna, G. J. Reversible Multiple Time Scale Molecular Dynamics. *J. Chem. Phys.* **1992**, 97 (3), 1990–2001.

55. Plimpton, S. Fast Parallel Algorithms for Short-Range Molecular Dynamics. *J. Comput. Phys.* **1995**, *117* (1), 1–19.

56. Koga, K.; Tanaka, H.; Zeng, X. C. First-Order Transition in Confined Water between High-Density Liquid and Low-Density Amorphous Phases. *Nature* **2000**, *408* (6812), 564–567.

57. García Fernández, R.; Abascal, J. L. F.; Vega, C. The Melting Point of Ice Ih for Common Water Models Calculated from Direct Coexistence of the Solid–Liquid Interface. *J. Chem. Phys.* **2006**, *124* (14), 144506.

58. Pauling, L. The Structure and Entropy of Ice and of Other Crystals with Some Randomness of Atomic Arrangement. *J. Am. Chem. Soc.* **1935**, *57* (12), 2680–2684.

59. Luzar, A.; Chandler, D. Hydrogen-Bond Kinetics in Liquid Water. *Nature* **1996**, 379 (4), 55–57.

60. Nistor, R. A.; Markland, T. E.; Berne, B. J. Interface-Limited Growth of Heterogeneously Nucleated Ice in Supercooled Water. *J. Phys. Chem. B* **2014**, *118* (3), 752–760.

61. Imai, M.; Yokota, Y.; Tanabe, I.; Inagaki, K.; Morikawa, Y.; Fukui, K. I. Correlation between Mobility and the Hydrogen Bonding Network of Water at an Electrified-Graphite Electrode Using Molecular Dynamics Simulation. *Phys. Chem. Chem. Phys.* **2020**, *22* (3), 1767–1773.

62. Yang, J.; Meng, S.; Xu, L.; Wang, E. G. Water Adsorption on Hydroxylated Silica Surfaces Studied Using the Density Functional Theory. *Phys. Rev. B* **2005**, *71* (3), 1–12.

63. Smirnov, K. S. A Molecular Dynamics Study of the Interaction of Water with the External Surface of Silicalite-1. *Phys. Chem. Chem. Phys.* **2017**, *19* (4), 2950–2960.

64. Smit, W. J.; Tang, F.; Sánchez, M. A.; Backus, E. H. G.; Xu, L.; Hasegawa, T.; Bonn, M.; Bakker, H. J.; Nagata, Y. Excess Hydrogen Bond at the Ice-Vapor Interface around 200 K. *Phys. Rev. Lett.* **2017**, *119* (13), 133003.